

# A novel method based on Wiener filter for denoising Poisson noise from medical X-Ray images

Volkan Göreke

Sivas Vocational School of Technical Sciences, Department of Computer Technologies, Sivas Cumhuriyet University, 58140, Sivas, Turkey

## ARTICLE INFO

### Keywords:

Poisson noise  
X-ray image filter  
Artificial intelligence

## ABSTRACT

**Background and Objective:** The Poisson noise is added to the image during the acquisition of medical X-Ray images. The distorted image due to this noise makes it difficult for physicians to diagnose the disease. Although there are various approaches for filtering Poisson noise, these approaches have disadvantages such as excessive smoothing of the image, distorting the texture information, reducing the image quality and high computational cost. In this study, a novel method that removes Poisson noise from medical X-Ray images is proposed by overcoming the above mentioned disadvantages.

**Methods:** In the proposed method, the Wiener filter is modified using the FIR filter embedded in the standard Wiener algorithm. The FIR filter design was carried out using the ASO optimization algorithm. Optimum local mean and optimum local variance values are calculated using the optimization matrix corresponding to the FIR filter coefficients and transferred to the standard Wiener filter layer as parameter inputs.

**Results:** The proposed method showed superior performance in synthetic images and medical X-Ray images in terms of PSNR, MSE, SSIM metrics and image quality metrics such as luminous intensity, Contrast index, Entropy and Sharpness. The time consumption of the proposed method is much less.

**Conclusions:** The clinical usage of the proposed method may help doctors to be able to diagnose the disease more accurately by interpreting the X-ray images. Besides, the proposed method can also have a positive effect on the CAD performance by using it at the pre-processing stage of CAD systems.

## 1. Introduction

Medical imaging systems have an important role in the diagnosis processes of doctors. Using medical images, the doctors have information about the internal parts of the body and the organs [1]. Through medical images which are different from other image types in terms of the information obtained by pixels, the doctors can diagnose the complex diseases much more accurately [2]. Different types of imaging techniques are used for the different parts of the human body. X-ray imaging is a technique that is mostly used at the regions between the bones and the tissue around the bones [3].

The undesirable components that affect the image data due to various reasons, are called noise. Basically, there are four types of noise encountered in medical images. These are Gaussian Noise, Salt and Pepper Noise, Speckle Noise and Poisson Noise. Gauss noise is usually caused by sensors or low illumination [4]. Salt and Pepper Noise occurs because of the transmission and scanning of images. Such kind of a noise has an effect of randomly scattered inverse pixels [5]. Speckle Noise depends on the imaging device. The phase sensitivity of the transducers

causes such kind of a noise [6]. X-Ray imaging is both very popular in medical fields and it has a low cost. X-rays are obtained using photons smaller than 0.2 nm wavelength [7]. The X-rays obtained in the producer system reach the receiver system by scattering. This scatter follows the Poisson distribution [8]. This behavior of X-rays affects the grey levels of an image as random values with Poisson distribution and is called the Poisson noise. The magnitude of the noise is directly proportional to the ray amplitude [9].

For example, in mammography images, the statistical behavior of electromagnetic wave in X-Ray causes poisson noise [10].

The doctors may have difficulties in the diagnosis because of the noise that naturally exist in the medical images. The Poisson noise in the X-ray images prevent the detection of coughing and capillary fractures in the bones and it must be eliminated [11,12]. Usually, the filtering techniques are used to eliminate the noise in the medical images [13]. Various filtering techniques that reside in the scope of this study are summarized in Section 2.

The standard Wiener filter is a method used in the field of image filtering [14]. Cannistraci et al. modified the standard Wiener filter to

E-mail address: [vgoreke@cumhuriyet.edu.tr](mailto:vgoreke@cumhuriyet.edu.tr).

<https://doi.org/10.1016/j.bspc.2022.104031>

Received 19 April 2022; Received in revised form 11 July 2022; Accepted 26 July 2022

1746-8094/© 2022 Elsevier Ltd. All rights reserved.

remove speckle noise [15]. They used local median instead of local mean in their proposed method. They named their proposed method as “Median-modified Wiener filter” (MMWF).

Park and Lee used the MMWF technique for noise removal from breast phantom images [16]. Park et al. used the MMWF method to improve the quality of gamma camera images [17]. In a recent study, Xie et al. proposed a new Wiener filter based on field pattern analysis to improve the quality of ultrasound images [18]. In our study, the Wiener filter was modified by developing a different technique than the above methods.

Although it is out of the scope of this study, image filtering is also included in the current studies in the literature as a preprocessing step in studies such as nodule detection and segmentation. For example, Rauf et al. used the standard Wiener filter in their study of Lung nodule detection and removed noise from computed tomographic images [19]. İrfan et al. used size filter to filter the noise in the segmentation study of breast ultrasound images [20]. Meraj et al. proposed a U-Net approach for segmentation of breast lesions. In their study, they filtered the noisy image dataset by a Gaussian filter [21].

Optimization algorithms are an artificial intelligence technique that is frequently used in various medical image processing studies. In his current studies, Dinh has used new optimization algorithms such as Grasshopper optimization algorithm (GOA), Equilibrium optimizer Algorithm (EOA), Marine predators algorithm (MPA) in fields such as medical image fusion [22 23 24 25 26 27 28].

Additionally, removal of noise from the images has also a positive effect on the performance of the computer-aided diagnostic (CAD) systems [29].

The aim of this study is to propose a novel and effective filter structure that eliminates the disadvantages of the methods proposed in the literature, such as excessive softening, loss of texture features, reduction in image quality and excessive computation time.

In this study, a novel method based on the Wiener filter is proposed for denoising the Poisson noise in X-Ray images. This study is within the scope of reducing the poisson noise of x-ray images in the medical field. In the proposed method, a 2D finite impulse response (FIR) filter was designed that works within the classical Wiener algorithm. Optimum local mean and optimum local variance values were obtained using FIR filter coefficients and they were transmitted to Wiener algorithm as parameter inputs. FIR filter coefficients were obtained using an artificial intelligence search algorithm called Atom search. The performance of the proposed method in terms of various metrics, was compared with classical filters and different approaches in the literature. The results show that the proposed method has better performance than both classical filters and the other approaches in the literature.

The paper is organized as follows. In Section 2, the common methods in the literature were summarized. In Section 3, the software platform and dataset were introduced first. Then the details of the method were given with the mathematical background. In Section 4, the performance of the proposed method was compared with the literature; numerical and graphical results were provided. Section 5 is the conclusion and discussion session.

## 2. Literature review

In the literature, there are several approaches to remove Poisson noise from X-ray images, such as filters, wavelet-based methods, hibrit (spatial domain and transform domain), machine learning and deep learning. Kirti et al. aimed to remove the Poisson noise from X-Ray images by using Harris detector and responsive median filter in spatial domain. Besides, they compared the Peak signal-to-noise ratio (PSNR) performance of their work with moving average filter, Non-Local Mean (NLM) and Block Matching and 3D filtering (BM3D) techniques document[7]. Subbuthai et al. mentioned that the median filter had performed better than Gaussian filter for filtering the Poisson noise in medical X-Ray images [30]. However, in this approach the subtle texture

details can not be distinguished from the noise and filtered [11]. The bilateral filter introduced by Tomasi and Manduchi, uses the photometric and geometric similarities of the near neighborhood pixels to estimate pixel values [31]. However, the bilateral filter causes gradient inverse artifact that generates unstable weighted average in the neighborhood of similar pixels [11]. Thakur et al. applied Poisson noise filtering on medical X-Ray images in their study which depends on bilateral filter approach [12]. Asim et al. compared the Poisson noise filtering performances of Dual-tree Complex Wavelet Transform (DTCWT), Non-Local Mean (NLM) and Wiener filter together with bilateral filter [32]. In Non-Local Mean (NLM) filtering method introduced by Buades, the weighted average of the pixels in the image is calculated according to the similarity to the target pixel [33]. Irreta et al. had an approach using the adaptive NLM method to reduce the Poisson noise in the medical X-Ray images [34].

The Guided filter, based on a local linear model, was presented by He et al. [35]. In this technique, filtering is done by referencing the content of a guide image. Zhang and He performed image filtering studies using Guide filter on non-medical images [36]. In the study of Chandra and Verma, poisson noise was filtered from medical X-Ray images using different filter structures. They compared their results using metrics such as MSE and PSNR. According to this study, The Guided filter and the Bilateral filter had very close performance [11].

The Bayes shrink method proposed by Chang et al. uses wavelet soft-thresholding technique. The threshold that is used in the wavelet coefficients is constructed via Bayesian Framework and has an adaptive structure [37]. However, the image quality decreases in methods with thresholding because the texture information can not be preserved appropriately. Soft-thresholding generates more errors than hard-thresholding [38]. Thus, in this study the Bayes shrink method was compared with the method that contains hard thresholding. Ling Wang et al. used Bayes shrink filtering technique and adaptive median filter to reduce Poisson noise at medical X-Ray images [39]. Ling Wang et al. used X-Ray images with different doses and applied Bayes shrink method with Wiener filter to reduce Poisson noise [8].

Du et al. showed that the performance of the dual tree complex wavelet transform (DTCWT) was better than wavelet transform for reducing the Poisson noise in X-Ray images [40].

Ferrari and Winsor applied a method that contains DTCWT to remove the Poisson noise from digital radiographic images. They filtered the medical X-Ray images and compared the performance of the proposed method with Gaussian filter method in terms of PSNR metric [41].

Luisier et al. proposed PURE-LET (Poisson Unbiased Risk Estimation – Linear Expansion of Thresholds) method to reduce the Poisson noise. This method is based on minimizing the Poisson unbiased risk estimate and uses the linear expansion of thresholds [42]. The disadvantage of this method is that it causes artifacts [43].

A hybrid method in the literature is the state-of-the-art method called “block matching and 3D filtering” (BM3D) that was proposed by Dabov et al [44]. The disadvantage of this method is to modify the texture information significantly by heavily softening the image [45]. The preservation of texture features affects the classification performance of disease detection systems [11]. Lee and Kang used a method like BM3D to reduce the Poisson noise in X-Ray images. Furthermore, they evaluated the Poisson noise reduction performance of PURE-LET method in the medical X-Ray images in terms of peak signal-to-noise ratio (PSNR) metric [46].

Dual-tree Complex Wavelet Transform (DTCWT) which was introduced by Kingsbury, is a method that depends on wavelet transformation. In this method, two trees are used in which the imaginary and real parts of the wavelet coefficients are generated [47].

In some of the approaches in the literature, initially the noise is transformed into an approximately Gaussian distribution. This transformation is realized by applying variance stabilization transform (VST) [48]. After the transformation, a filtering method for Gaussian noise is applied to the image. The final image is obtained using an inverse

transformation. Additionally, in the case of low signal-to-noise ratio, the performance of the methods based on VST is lower than the methods that deal with the Poisson noise directly [49]. Hai et al. introduced an algorithm using VST method to filter the Poisson noise in medical X-Ray images [50].

Spars-based methods, which is a machine learning technique, were used in the field of image filtering [51]. The origin of the Sparse representation is based on the compressed sensing technique proposed by Donoho [52]. According to this technique, the original signal can be reconstructed using several measured sampling values [53]. The sparse representation has been used in computer vision, face recognition, action recognition, object tracking and image denoising studies in recent years [54]. Elad and Aharon used the sparse representation technique to remove Gaussian noise in non-medical images [55]. Giryes and Elad presented a sparsity-based method to remove the Poisson noise from non-medical images [56]. Although sparse-based methods have good filtering performance, they can involve a complex and iterative optimization problem. This problem causes the filtering process to be prolonged and reduces its practical applicability.

A locally adaptive regression kernel image denoising (LARK) filter technique was presented by Takeda et al. to remove Gaussian noise from the image. The technique they present is an extension of the bilateral filter [57]. According to the study of Zhu and Yu, LARK technique showed a lower performance than NLM technique in removing Gaussian noise [58].

Image filtering studies using deep neural network were first performed by Liang and Liu in 2015 [59]. Mao et al. designed a deep network-based framework for image filtering [60]. Zang et al. proposed a deep convolutional neural network structure to remove Gaussian noise [61]. Jia et al. proposed a deep convolutional neural network structure for image filtering [62]. Lyu et al. performed a Gaussian noise removal study by integrating the nonsubsampling shearlet transform structure into the convolutional neural network structure [63]. Song et al used cascaded multi-supervision convolutional neural networks to remove noise from Magnetic resonance and Computed Tomography images [64].

Although deep neural networks are successful in removing noise, they also have some important disadvantages. Deep neural networks require a lot of memory resources and computational costs. Training the network for real noisy images is not a stable solution. Deep neural networks have difficulty solving the problem of unsupervised noise removal. [51].

### 3. Material and method

In this study, a novel method was introduced to filter the Poisson noise from medical X-Ray images where a 2D FIR filter was nested in the standard Wiener algorithm. Optimization algorithms, an artificial intelligence application, were used for 2D FIR filter design. In the current study of Chandra et al., filtered images were classified using different filter structures by the ANN classifier [11]. Taking this study as a reference, the Wiener filter, which is the most successful on average, was used in this study.

The synthetic images generated by computer were used to develop the proposed method. The performance of the proposed method was initially compared with the standard filters that use synthetic images. Then it was compared with the methods in the literature in terms of various metrics using many medical X-Ray images. The system design and performance evaluation processes were implemented as a software in MATLAB 2016a IDE environment.

The URLs of the medical X-Ray images that were used in the study are as follows.

For chest X-Ray images: <https://www.kaggle.com/tawsifurrahman/covid19-radiography-database> For hand and breast images: [https://www.imageprocessingplace.com/DIP-3E/dip3e\\_book\\_images\\_downloads.htm](https://www.imageprocessingplace.com/DIP-3E/dip3e_book_images_downloads.htm).

<https://www.kaggle.com/prashant268/chest-xray-covid19-pneumonia>.

#### 3.1. Mathematical background

The Wiener filter is used to estimate the pixel value using the local pixel average and standard deviation of the neighboring pixels. Although it is a classical approach for denoising, it is accepted as an optimum filter for minimum mean squared error (MSE) [65]. For the standard Wiener filter, the local mean value  $\mu$  and the local standard deviation value  $\sigma$  for the pixel at the location  $(i,j)$  of the image  $P$  are given in Equation 1 and Equation 2 respectively where the dimensions of filter kernel are  $(2M+1) \times (2N+1)$  [66].  $P'$  represents the filtered image matrix and the mathematical equation of the pixel value at the location  $(i,j)$  is given in Equation 3. Here  $\sigma_n$  is the variance of the noise. If the variance of the noise is not given, Wiener uses the average of all the local estimates of the variances.

$$\mu(i,j) = \frac{1}{((2M+1) \times (2N+1))} \sum_{m=-M}^M \sum_{n=-N}^N P(i+m,j+n) \quad (1)$$

$$\sigma(i,j) = \sqrt{\frac{1}{((2M+1) \times (2N+1))} \sum_{m=-M}^M \sum_{n=-N}^N P^2(i+m,j+n) - \mu^2(i+m,j+n)} \quad (2)$$

$$P'(i,j) = \mu(i,j) + \frac{\sigma(i,j)^2}{\sigma(i,j)^2 + \sigma_n^2} (P(i,j) - \mu(i,j)) \quad (3)$$

In this study, instead of classical local mean and local standard deviation, a calculation method for optimum local mean and optimum local standard deviation was given. In the proposed method,  $C_{mn}$  represents the kernel matrix that contains the optimization coefficients. The equations for calculating optimum local mean and optimum local variance can be rearranged as Equation 4 and Equation 5.

$$\mu_{opt}(i,j) = \frac{1}{((2M+1) \times (2N+1))} \sum_{m=-M}^M \sum_{n=-N}^N C_{mn}(m,n)P(i+m,j+n) \quad (4)$$

$$\sigma_{opt}(i,j) = \sqrt{\frac{1}{((2M+1) \times (2N+1))} \sum_{m=-M}^M \sum_{n=-N}^N C_{mn}(m,n)P(i+m,j+n)^2 - \mu_{opt}^2} \quad (5)$$

As an example, for an optimization kernel of size  $3 \times 3$ ,  $C_{mn}$  is represented with a matrix given in Equation 6. Equation 6 is a mathematical notation that denotes the filter kernel [65]. In Equation 6, the  $C$  values represent the FIR filter coefficients to be obtained using the optimization algorithm.  $m, n$  indicates the pixel location of these coefficients [65]. Here  $m, n \in \{-1,0,1\}$ .

$$C_{mn} = \begin{bmatrix} C_{-1,-1} & C_{-1,0} & C_{-1,1} \\ C_{0,-1} & C_{0,0} & C_{0,1} \\ C_{1,-1} & C_{1,0} & C_{1,1} \end{bmatrix} \quad (6)$$

In linear spatial filtering operations, there are two closely related concepts called correlation and convolution. Convolution operation is achieved by rotating the filter matrix of the correlation operation 180 degrees [67]. Commonly convolution is used in the literature. Therefore, the convolution method was preferred in this study.

The mathematical equivalent of  $\sum_{m=-M}^M \sum_{n=-N}^N C_{mn}(m,n)P(i+m,j+n)$  in Equation 4 corresponds to the correlation operation [68]. The correlation operation corresponds to the convolution if the  $C_{mn}$  matrix is rotated 180 degrees [67]. Thus, Equation 4 and Equation 5 can be given as Equation 7 and Equation 8.

$$\mu_{opt} = \frac{1}{((2M+1) \times (2N+1))} (C'_{mn} * P) \quad (7)$$

**Table 1**  
Minimization performances of popular optimization algorithms.

Algorithms	PSO [69]	HARMONY [70]	GA [71]	ABC [72]	CSA [77]	EOA [74]	GOA [75]	MPA [76]	ASO [73]
Best	21,67116	24,42495	24,41835	25,97930	24,21835	18,81200	18,8700	19,9474	<b>18,70384</b>
Worst	22,69576	25,19169	25,21512	26,94662	25,14212	19,98700	20,7977	20,6534	<b>19,66099</b>
Mean	22,26023	24,77300	24,78945	26,37040	24,10945	19,70960	19,8259	19,9814	<b>19,26286</b>
Std	0,246907	0,247609	0,243547	0,242320	0,242545	0,242230	0,24750	0,28360	<b>0,242115</b>

```

Randomly initialize a set of atoms  $X$  (solutions), velocity  $v$ ,  $Fit_{best} = Inf$ 
While the stop criterion is not satisfied do
  For each atom  $X_i$  do
    Calculate the fitness value  $Fit_i$ ;
    If  $Fit_i < Fit_{best}$  then
       $Fit_{best} = Fit_i$ ;
       $X_{best} = X_i$ ;
    End If
  Calculate the mass using Equations 10 and 11 ;
  Determine its  $K$  neighbors using Equation 12;
  Calculate the interaction force  $F_i$  and constraint force  $G_i$  using
  Equations 13 and 14 ;
  Calculate the acceleration using Equation 15;
  Update the velocity using Equation 16;
  Update the position using Equation 17;
End For
End While
Find the solution so far  $X_{best}$ 

```

**Fig. 1.** Pseudo code for ASO.

$$\sigma_{opt} = \sqrt{\frac{1}{((2M + 1) \times (2N + 1))} (C_{mn} * P^2) - \mu_{opt}^2} \quad (8)$$

In Equation 7 and Equation 8  $\mu_{opt}$  and  $\sigma_{opt}$  represent the matrices that contain the optimum mean and optimum standard deviation values of image matrix P at location (i,j).

Using the proposed method, the value of the pixel at the filtered location (i,j) can be rearranged as Equation 9.

$$P'_{opt}(i,j) = \mu_{opt}(i,j) + \frac{\sigma_{opt}(i,j)^2}{\sigma_{opt}(i,j)^2 + \sigma_n^2} (P(i,j) - \mu_{opt}(i,j)) \quad (9)$$

Here  $C_{mn}$  matrix is the 180 rotated version of  $C_{mn}$  matrix.

$(C_{mn} * P)$  represents the 2D convolution between  $C_{mn}$  matrix and P matrix. In this study, a two-dimensional filter application was realized by applying the convolution operation and linear shift invariant technique to the image matrix [69]. The optimization matrix was obtained by calculating the suitable coefficients (the elements of  $C_{mn}$  matrix) for the system zeros of the designed FIR filter.

### 3.2. The proposed filter architecture and adaptive 2D FIR filter design

In the requirements analysis stage for FIR filter, usually the frequency domain is preferred. The system response is determined using the zeros of the transfer function. Usage of optimization algorithms to calculate the suitable coefficients for the system zeros, takes part in the literature [13].

The suitable coefficients for the system zeros of the FIR filter designed in this study (the elements of  $C_{mn}$  matrix) were obtained with an experimental study where the popular optimization algorithms were individually tested.

The algorithms were structured as they would search for suitable solutions which would minimize the fitness function in the problem space. For each algorithm, the mean square error (MSE) given in Equation 18 was used as the fitness function. The mean square of the

difference between the density values of the original images and the denoised images is called the MSE where the low MSE is a measure of high performance [70]. In the experimental study, every algorithm was run for twenty times and the best, the worst, mean and standard deviation values were shown in Table 1.

The algorithms used in this study can be summary as follows.

Particle Swarm Optimization (PSO) [71], Harmony Search Algorithm (Harmony) [72], Genetic Algorithm [73], Artificial Bee Colony (ABC)[74], Atom Search Optimization (ASO)[75], Equilibrium Optimization Algorithm (EOA) [76], Grasshopper Optimisation Algorithm (GOA) [77], Marine Predators Algorithm (MPA) [78], Crow Search Algorithm (CSA) [79].

The best performance was obtained by Atom Search Optimization (ASO) in the experimental study. ASO was introduced by Zhao et al. in 2019 where the molecular dynamics were referenced. ASO mathematically models the atomic motion resulting from the interaction of the atoms in the nature with the effect of two forces. The forces that affect the atoms are the interaction forces resulting from Lennard-Jones potential and constraint forces resulting from bond-length potential [75]. The pseudocode for ASO algorithm is shown in Fig. 1.

Equation 10 and Equation 11 are used to calculate the mass of the  $i$ th atom.

$$M_i(t) = e^{-\frac{Fit_i(t) - Fit_{best}(t)}{Fit_{worst}(t) - Fit_{best}(t)}} \quad (10)$$

$$m_i(t) = \frac{M_i(t)}{\sum_{j=1}^N M_j(t)} \quad (11)$$

$K$  refers to the neighbors with higher fitness values with which each atom interacts. Its mathematical expression is given by the Equation 12.

$$K(t) = N - (N - 2) \times \left(\frac{t}{T}\right)^{0.5} \quad (12)$$

$F$  is the total effect on the  $i$ th atom of random weights originating from other atoms.

Its mathematical expression is given by the Equation 13.

$$F_i^d(t) = \sum_{j \in K_{best}} rand_j F_{ij}^d(t) \quad (13)$$

$G$  is the constraint force and is defined by Equation 14.

$\lambda(t)$  is the Lagrangian multiplier.

$$G_i^d(t) = \lambda(t)(x_{best}^d(t) - x_i^d(t)) \quad (14)$$

The acceleration of the atom  $i$ th at time  $t$  is calculated by Equation 15.

$$a_i^d(t) = \frac{F_i^d(t) + G_i^d(t)}{m_i^d(t)} \quad (15)$$

In the  $(t + 1)$ th iteration, the velocity and position of the  $i$ th atom are calculated using Equation 16 and Equation 17.

$$v_i^d(t + 1) = rand_i^d v_i^d(t) + a_i^d \quad (16)$$

$$x_i^d(t + 1) = x_i^d(t) + v_i^d(t + 1) \quad (17)$$

In the ASO algorithm shown in Fig. 1,  $X$  atoms represent the elements



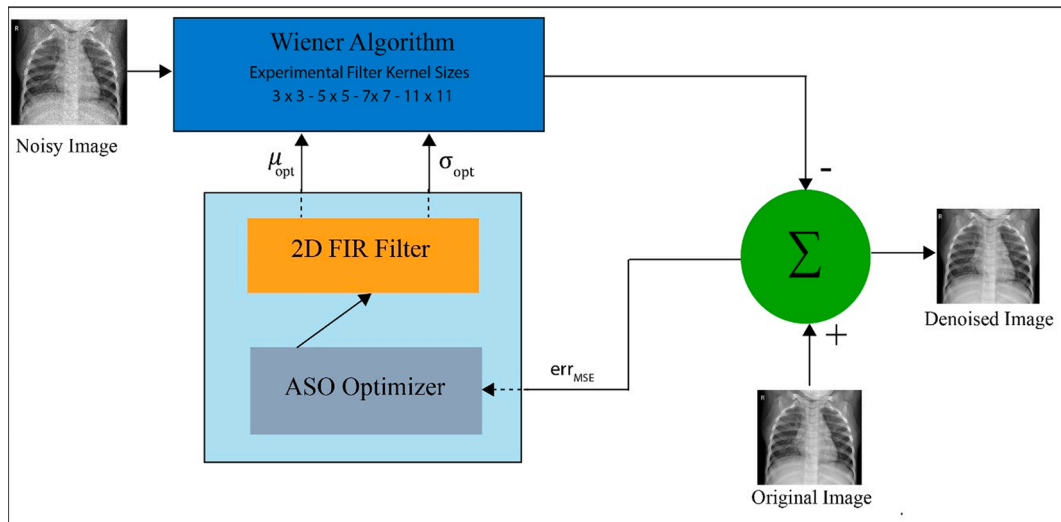


Fig. 2. The block diagram of the filter architecture for the proposed method.

Table 2  
P-values from Wilcoxon rank-sum.

Compared Algorithms	P-values
ASO-PSO	6,2918E-8
ASO-HARMONY	6,2816E-8
ASO-GA	6,2818E-8
ASO-ABC	6,2718E-8
ASO-CS	6,2715E-8
ASO-EOA	1,4215E-6
ASO-GOA	1,4212E-6
ASO-MPA	1,4232E-6

Table 3  
PSNR (dB) performance comparison of synthetic image standard filtering techniques.

Peakvalue	Noisy Image	Moving Average [78]	Median [79]	Wiener [14]	Proposed Method
255	27.5507	30.7184	34.5801	35.1794	<b>35.4014</b>
100	17.4199	18.5876	26.5283	27.1262	<b>27.1584</b>
50	11.3993	12.5670	20.4500	21.0697	<b>21.0947</b>

Table 4  
MSE-SSIM performance comparison of standard filtering techniques for synthetic images.

Metric	Noisy Image	Moving Average [78]	Median [79]	Wiener [14]	Proposed Method
MSE	114.4201	34.4319	22.6503	19.2815	<b>18,70384</b>
SSIM	0.4434	0.8078	0.8159	0.8498	<b>0.8577</b>

of the optimization matrix  $C_{mn}$  which will be searched in the problem space. The  $X$  atoms (elements of the  $C_{mn}$  matrix) are initially randomly generated by the algorithm. The Fit variable represents the fitness function. In the proposed method, the MSE value between the noisy image and the filtered image is used as the Fitness function. This function was expressed as  $err_{MSE}$  in Fig. 2.

For the experimental study, noisy synthetic image  $P$  was obtained by adding the Poisson noise to the synthetic image  $P_{org}$  that was generated in the computer. All optimization algorithms used in this study searched for the optimization matrix that would minimize the fitness function. The filter architecture proposed in this study is shown in Fig. 2. The Wiener algorithm is given with Algorithm 1 [14].

Algorithm 1. The Wiener filter algorithm

For each pixel in the image Do  
 Step 1. Determine filter kernel,  $M$  (row size) and  $N$  (column size)  
 Step 2. Calculate local mean around each pixel using Equation 1  
 Step 3. Calculate standard deviation around each pixel using Equation 2  
 Step 4. Calculate filter output using Equation 3  
 End Do

$$MSE = \frac{1}{M \times N} \sum_{i=1}^M \sum_{j=1}^N (P_{org}(i,j) - P'(i,j))^2 \quad (18)$$

Here  $P_{org}$  and  $P'$  represent the original and the filtered images respectively.

An experimental study was conducted to determine the most performant filter window sizes frequently encountered in the literature [13]. In the experimental study, noise suppression and preservation of visual details were taken into account.

In the experimental study, various sizes of optimization kernels such as  $3 \times 3$ ,  $5 \times 5$ ,  $7 \times 7$ , and  $11 \times 11$  were used and the kernel with size  $3 \times 3$  had the best performance. Steps of the proposed method are given in Algorithm 2.

In the literature, non-parametric tests were used to compare the performances of algorithms [24]. In this study, the performances of the algorithms were tested using the Wilcoxon rank-sum, and the results are given in the Table 2. Since the results (p values) given in the Table 2 are less than 0.05, the results are statistically significant.

In the proposed method, the performance of the optimization algorithm directly affects the performance of the filter to be designed. because the coefficients of the FIR filter embedded to the Wiener algorithm are obtained by using the optimization algorithm.

Each of these algorithms was run twenty times to determine the most successful algorithm. The best and worst values in Table 1 are the MSE values obtained by each algorithm in 20 runs. The mean value is the average of 20 study results. According to these values, the lowest MSE

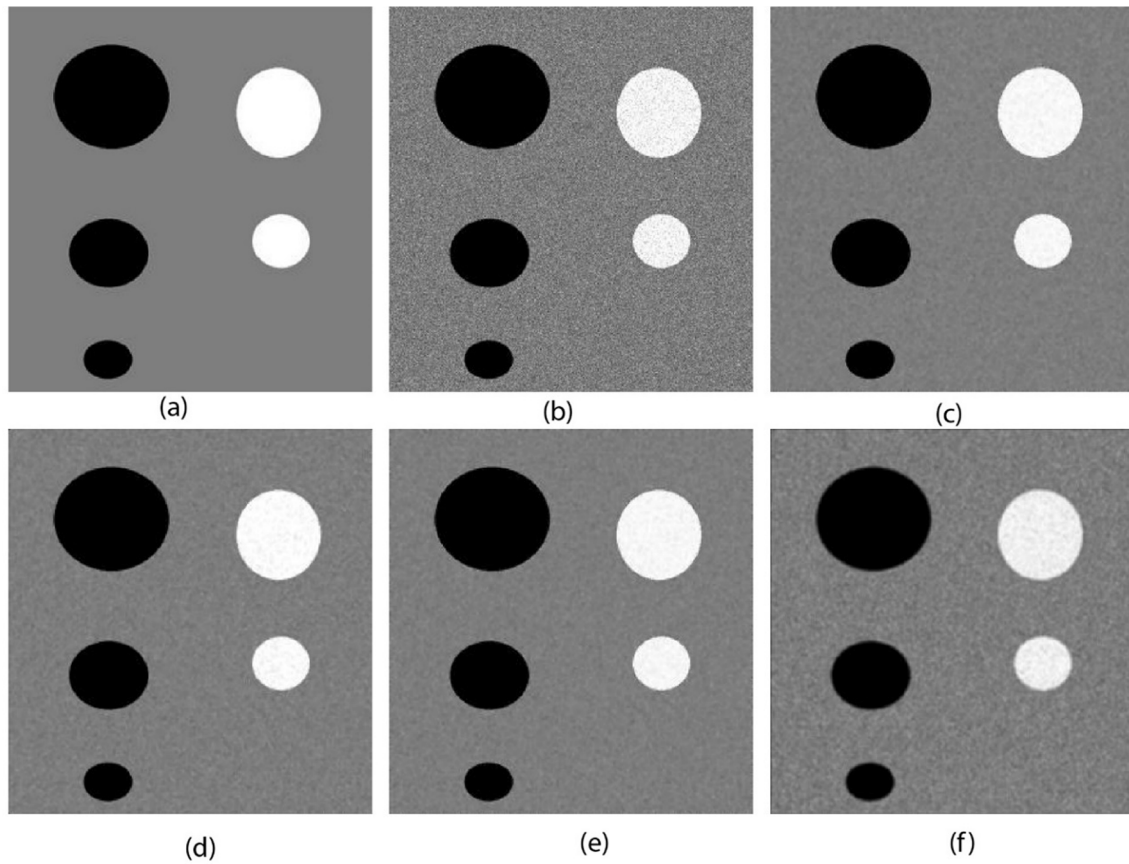


Fig. 3. a) Original synthetic image, b) Image with noise, c) Image filtered with the proposed method, d) Image filtered with the median filter, e) Image filtered with the Wiener filter, f) Image filtered with the moving average.

Table 5  
PSNR (dB) filtering performances for various noisy medical X-Ray images.

Metric	Noisy Image	Bilateral Filter [29]	NLM [31]	BM3D [42]	PURE-LET [40]	DTCWT [45]	Bayes Shring [35]	Proposed Method
PSNR								
Cheast	27.2467	33.5003	33.6004	34.1189	34.0800	32.9706	32.0383	<b>34.2000</b>
Hand	31.1240	33.7576	34.8036	35.9825	35.5588	34.3313	35.4180	<b>36.0162</b>
Breast	29.9476	32.4013	34.0639	35.1333	35.5660	34.8995	34.3624	<b>35.5727</b>

Table 6  
MSE filtering performances for various noisy medical X-Ray images.

Metric	Noisy Image	Bilateral Filter [29]	NLM [31]	BM3D [42]	PURE-LET [40]	DTCWT [45]	Bayes Shring [35]	Proposed Method
MSE								
Cheast	122.2845	51.7459	31.5039	25.2736	28.9301	26.0430	40.3845	<b>25.0455</b>
Hand	50.1973	27.3727	21.6819	16.3996	18.0802	17.4190	18.9381	<b>16.3202</b>
Breast	65.8142	37.4066	25.5912	20.0064	18.0500	21.5954	23.8146	<b>18.0379</b>

Table 7  
SSIM filtering performances for various noisy medical X-Ray images.

Metric	Noisy Image	Bilateral Filter [29]	NLM [31]	BM3D [42]	PURE-LET [40]	DTCWT [45]	Bayes Shring [35]	Proposed Method
SSIM								
Cheast	0.6061	0.8266	0.8722	<b>0.9057</b>	0.8409	0.8696	0.8193	0.9004
Hand	0.7337	0.8336	0.9177	0.9245	0.9104	<b>0.9249</b>	0.8977	0.9219
Breast	0.6336	0.7749	0.8498	0.8751	<b>0.9037</b>	0.8973	0.8420	0.8965

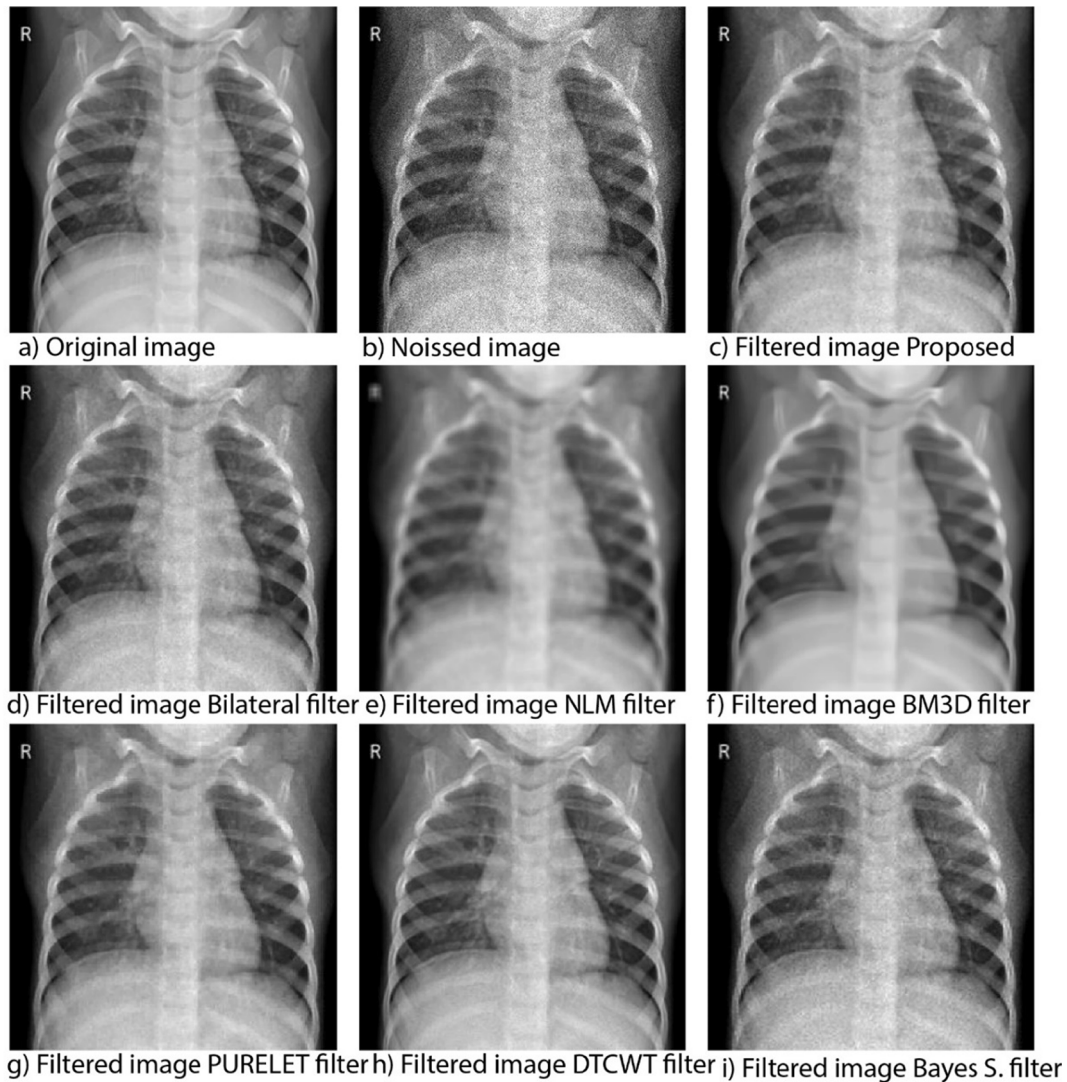


Fig. 4. Chest X-Ray filtered with various methods in the literature.

was obtained by the ASO algorithm. In addition, ASO can produce values closer to the mean (low standard deviation).

Algorithm 2. Steps of the proposed method

```

Begin
1. Read image  $P_{org}$ 
2. Add poisson noise to  $P_{org}$  generate noisy image  $P$ 
3. Apply zero padding [67] to  $P$  image
4. Apply ASO optimization:
  a. Define population size  $N$ ,  $N = 30$ 
  b. Define lower limit  $Lower\_L$ , upper limit  $Upper\_L$  vector
      $n = row\_size(optimization\ kernel) \times column\_size(optimization\ kernel)$ ;
      $Lower\_L = [LL1, \dots, LLn]$ ,  $\forall LL \in \{0.9\}$ 
      $Upper\_L = [UL1, \dots, ULn]$ ,  $\forall UL \in \{1.2\}$ 
     Define stopping criteria Max iteration,  $Max\_iteration = 300$ 
  c. Define fitness function using Equation 18
  d. Find  $\mu_{opt}$ ,  $\sigma_{opt}$  matrix using Equation 7, Equation 8
5. Calculate  $\sigma_n^2$ 
6. For  $i = 1$  to  $size(P(row\_size))$  Do
   For  $j = 1$  to  $size(P(column\_size))$  Do
     Calculate  $P_{opt}(i,j)$  using Equation 9
   End For
End For
End Begin

```

The optimization matrix obtained with the proposed method is given in Equation 19. Equation 19 denotes the FIR filter coefficients (elements of

the  $C_{mn}$  matrix) designed using the ASO optimization algorithm (Starts at step 4 in the Algorithm 2). In the optimization process, the ASO algorithm searches FIR filter coefficients that minimize the MSE error. These coefficients obtained at the end of the optimization process represent the elements of the  $C_{mn}$  matrix.

$$C_{mn}^i = \begin{bmatrix} 1.0012 & 1.0018 & 1.0021 \\ 0.9994 & 1.0011 & 1.0014 \\ 1.0090 & 0.9894 & 0.9991 \end{bmatrix} \quad (19)$$

### 3.3. Performance comparison with standard techniques

Peak Signal-to-Noise ratio calculates the ratio of the peak signal to noise between two images in terms of decibels. This ratio is used as a measure of quality between the original and reconstructed image. As PSNR increases, the quality of the reconstructed image increases too [70]. The mathematical representation of PSNR metric is given in Equation 12. In the literature, Poisson noise was used with different peak intensity values to measure the performances of the methods for filtering the noise [12]. The performances of the proposed method and the methods in the literature used for Poisson noise filtering were measured with various peak intensity values and the results were given in Table 3. The standard filters used in this study are Moving Average [80], Median [81] and Wiener [14] filter techniques.

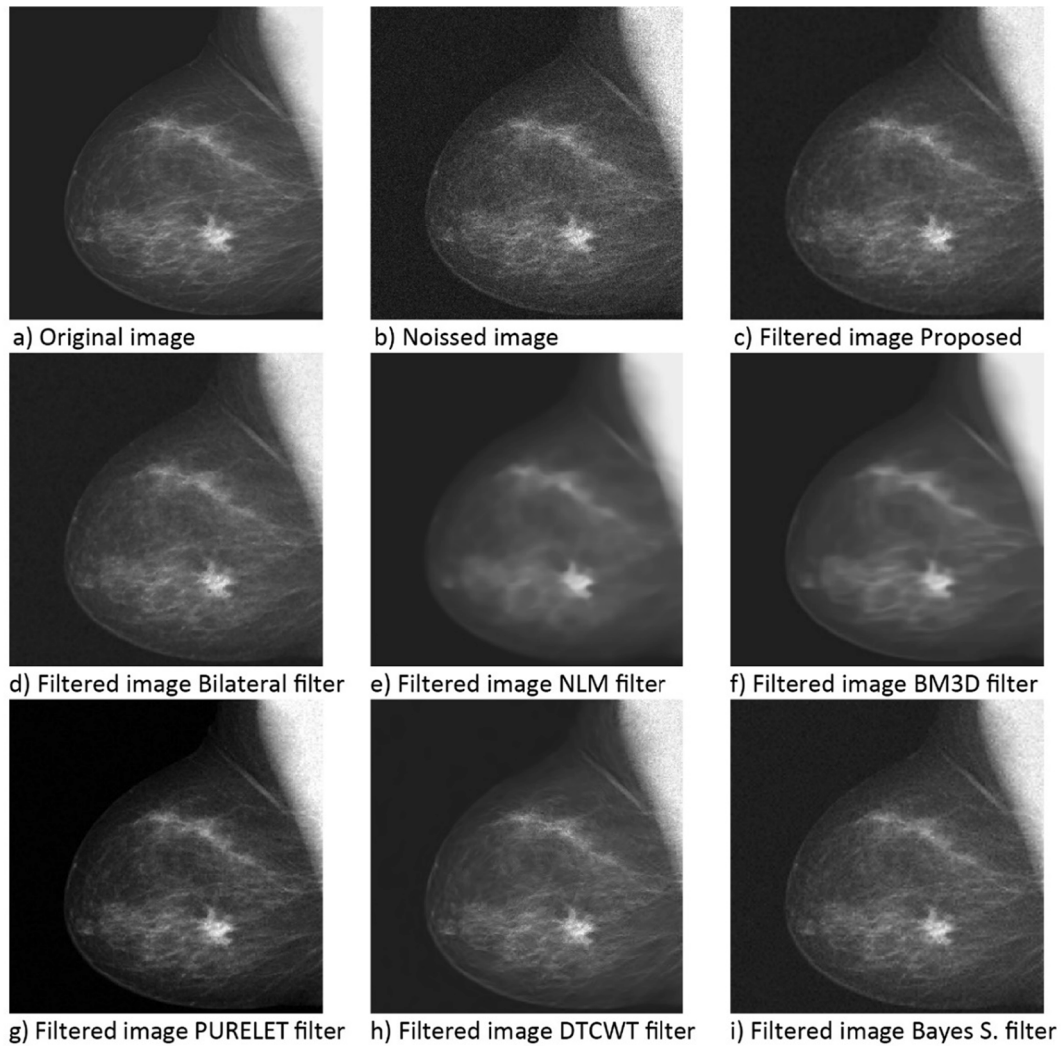


Fig. 5. Breast X-Ray image filtered with various methods in the literature.

Additionally, in this study performances were also compared using MSE and SSIM metrics and the results were given in Table 4. Structural similarity index (SSIM) is a measure of the similarity between two images. High SSIM indicates high performance in image filtering applications. [82]. Mathematical representation of SSIM is given in Equation 13.

$$PSNR = \frac{10 \times \log(I_g^2)}{MSE} \quad (12)$$

Here  $I_g$  represents the grey level in the image.

$$SSIM = \frac{(2\mu_x\mu_y + C_1)(2\sigma_{xy} + C_2)}{(\mu_x^2 + \mu_y^2 + C_1)(\sigma_x^2 + \sigma_y^2 + C_2)} \quad (13)$$

Here  $\mu$  is the mean,  $\sigma$  is the variance and  $\sigma_{xy}$  is the covariance.  $C_1$  and  $C_2$  are constants.

Visual outputs for application of noise reduction using standard filtering techniques and the proposed method are given in Fig. 3.

Considering the Table 3, the proposed method produced a superior result (high PSNR value) in suppressing noise for different peak values than standard filters. As seen in the Table 4, the proposed method provides lower filtering error (MSE) and higher structural similarity (SSIM). Table 3 and Table 4 show that the proposed method is more successful than the classical methods on the synthetic image in terms of the given performance metrics.

### 3.4. Limitations of the proposed method

The performance of the proposed method is closely related to the optimization algorithm used in the study. The limitation of the proposed method is that it has a fixed size kernel (Equation 19). This limitation creates a disadvantage against other methods. Equation 19 is a fixed matrix for all situations.

## 4. Clinical results

### 4.1. Performance comparison with different techniques in the literature

The performances of the proposed method and the approaches given in Section 2 for filtering the Poisson noise from the medical X-Ray images were compared using various X-Ray images and the results were given in Table 5, Table 6, and Table 7. The visual results of the X-Ray images filtered with the proposed method and various methods in the literature were given in Fig. 4, Fig. 5, and Fig. 6.

According to the results given in Table 5, Table 6 the proposed method had a better performance than all the other methods in the literature, in terms of PSNR and MSE metrics. The highest PSNR values and the lowest MSE values for three different x-ray images were obtained with the proposed method.

According to the results given in Table 7, in terms of the SSIM metric, it had very similar performances with BM3D, PURE-LET and DTCWT



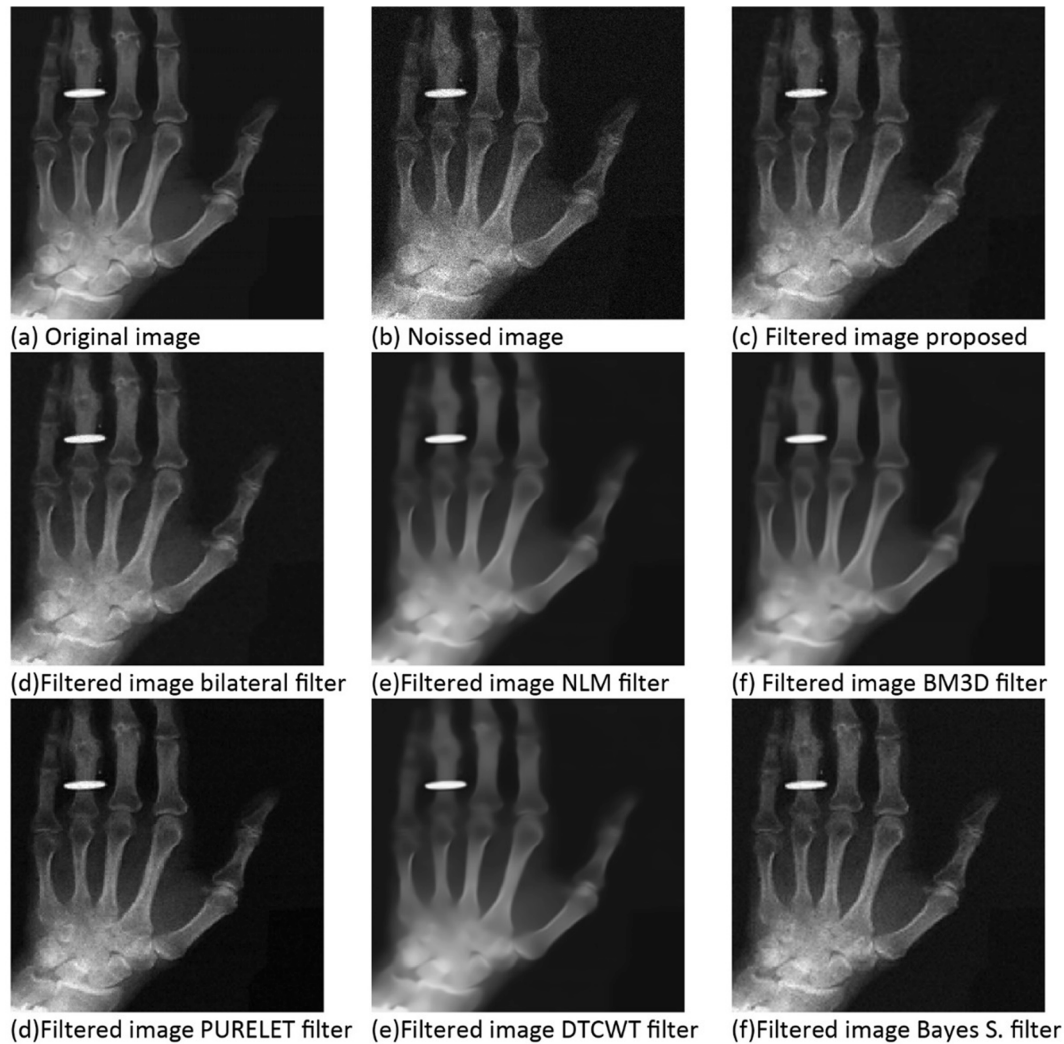


Fig. 6. Hand X-Ray image filtered with various methods in the literature.

Table 8

Performance comparison in terms of different metrics.

Method		ALI	CONTRAST	ENTROPY	SHARPNESS
Bilateral Filter [29]	Mean	0,5053	0,1451	7,5503	0,0234
	Std	0,0545	0,0242	0,1358	0,0026
NLM [31]	Mean	0,5056	0,0917	7,4540	0,0140
	Std	0,0548	0,0131	0,1358	0,0017
BM3D [42]	Mean	0,5052	0,1047	7,4618	0,0161
	Std	0,0547	0,0132	0,1391	0,0018
PURE-LET [40]	Mean	0,5060	0,1572	7,4348	0,0175
	Std	0,0552	0,0138	0,1336	0,0022
DTCWT [45]	Mean	0,5057	0,1550	7,5275	0,0232
	Std	0,0545	0,0530	0,1347	0,0046
Bayes Shring [35]	Mean	0,5056	0,1416	7,4594	0,0224
	Std	0,0549	0,0134	0,1383	0,0020
Proposed	Mean	<b>0,5105</b>	<b>0,1585</b>	<b>7,5072</b>	<b>0,0241</b>
	Std	0,0539	0,0129	0,1373	0,0018

Table 9

Time consumption comparison of the proposed method with other methods.

Method	Bilateral [29]	NLM [31]	BM3D [42]	PURE-LET [40]	DTCWT [45]	Bayes Shring [35]	Proposed
Time consumption (sn)	0,1348	5,7639	5,1796	0,3000	0,4317	0,8000	0,0627

methods in various medical X-Ray images. When these results were considered, it was demonstrated that the Poisson noise filtering performance of the proposed method in the medical images is superior to the methods in the literature.

There are also different metrics included in current studies in the literature for the measurement of image quality [24]. In addition, the performance of the proposed method in this study was evaluated using four different metrics. These are Average luminous intensity (ALI), Contrast index, Entropy and Sharpness, respectively. For the test applied at this stage, 200 images from the open access X-ray medical dataset were used (Dataset link: <https://www.kaggle.com/prashant268/chest-xray-covid19-pneumonia>). The results obtained are given in Table 8.

According to the results in Table 8, better quality images were obtained by the proposed method. For example, images obtained by other methods produced images with lower contrast than the proposed method.

The computer processing time required by the proposed method is given in Table 9 by comparing it with other methods.

As seen in the Table 9, the proposed method requires much less

computer processing time compared to other methods.

## 5. Discussion and conclusion

Reduction of Poisson noise is an image pre-processing stage and has a significant role on the diagnosis of the disease. In this study, a novel method was proposed for denoising the Poisson noise from medical X-Ray images. The proposed method contains the calculation of the optimum local mean and the optimum local standard deviation parameters instead of the local mean and local standard deviation parameters of Wiener algorithm. A software architecture was designed to be able to implement the proposed method where the standard Wiener algorithm and 2D FIR filtering algorithms were run nested. The matrix that contains the 2D FIR coefficients was named as the optimization matrix and was used in the calculation of optimum local mean and optimum standard deviation. The popular optimization algorithms were run for 20 times with kernels of size 3x3, 5x5, 7x7, and 11x11, and the ASO algorithm was chosen which had the best performance in terms of MSE metric. The performance of the system which was designed using synthetic images was compared with the classical filter structures in the literature in terms of MSE, PSNR and SSIM metrics and it had a better performance. The numerical results were given in Table 3 and Table 4. The visual results were given in Fig. 3.

The performance of the proposed method was compared with various approaches in the literature used for reducing the Poisson noise from medical X-Ray images in terms of MSE, PSNR and SSIM metrics, and the numerical results were given in Table 5, Table 6, and Table 7. The visual results of the medical images were given in Fig. 4, Fig. 5, and Fig. 6. The proposed method was able to reduce the Poisson noise in various types of medical X-Ray images in a superior way.

Although BM3D and NLM filters gave good results in Poisson noise suppression, they caused intense softening in the image. This softening effect is clearly seen in the visual results. Excessive softening causes texture features in the image to be lost [45]. Loss of the texture features adversely affects the classification performance of disease diagnostic systems [11].

The PURE-LET filter caused much less blur in the images. Considering this situation, PURE-LET filter showed the closest performance to the proposed method according to Bilateral, Bayes Shiring and DTCWT in noise suppression (PSNR value).

According to the results in Table 8, the proposed method in this study has higher ALI, Contrast, Entropy and Sharpness values. According to the results given in Table 8, our proposed method produces higher quality images.

Considering the Table 9, the computer processing time required by our proposed method is considerably less than other methods. In applications where a large number of images need to be filtered (for example, in deep learning-based classification problems), the proposed method provides a significant time advantage over other methods.

In addition, the use of the filter proposed in this study in the pre-processing stage of nodule detection and segmentation studies may contribute to these studies in a positive way.

It is considered that if the proposed method was applied to the clinical fields, the doctors would be able to diagnose the disease more accurately by interpreting the X-Ray images. The proposed method can transfer more accurate image information into the inputs of the CAD systems because it eliminates the noise more successfully. Thus, more accurate feature information can be obtained from the image information, and this may contribute to the performance of the system's decision support process.

As a future work, it is aimed to adapt the proposed method for different types of noises.

## Declaration of Competing Interest

The authors declare that they have no known competing financial

interests or personal relationships that could have appeared to influence the work reported in this paper.

## References

- [1] S.V. Mohd Sagheer, S.N. George, A review on medical image denoising algorithms, *Biomed. Signal Process. Control* 61 (2020), 102036, <https://doi.org/10.1016/j.bspc.2020.102036>.
- [2] L. Rundo, et al., MedGA: a novel evolutionary method for image enhancement in medical imaging systems, *Expert Syst. Appl.* 119 (2019) 387–399, <https://doi.org/10.1016/j.eswa.2018.11.013>.
- [3] W. Kong, Q. Miao, R. Liu, Y. Lei, J. Cui, Q. Xie, Multimodal medical image fusion using gradient domain guided filter random walk and side window filtering in framelet domain, *Inf. Sci. (Ny)* 585 (2022) 418–440, <https://doi.org/10.1016/j.ins.2021.11.033>.
- [4] C. Bonchelet, *Image Noise Models*, 1st ed., vol. 7. Elsevier, 2009. doi: 10.1016/B978-0-12-374457-9.00007-X.
- [5] S. Pyatykh, J. Hesser, Salt and pepper noise removal in binary images using image block prior probabilities, *J. Vis. Commun. Image Represent.* 25 (5) (2014) 748–754, <https://doi.org/10.1016/j.jvcir.2014.02.001>.
- [6] D. Li, W. Yu, K. Wang, D. Jiang, Q. Jin, Speckle noise removal based on structural convolutional neural networks with feature fusion for medical image, *Signal Process. Image Commun.* 99 (4) (2021), 116500, <https://doi.org/10.1016/j.image.2021.116500>.
- [7] T. Kirti, K. Jitendra, S. Ashok, Poisson noise reduction from X-ray images by region classification and response median filtering, *Sadhana - Acad. Proc. Eng. Sci.* 42 (6) (2017) 855–863, <https://doi.org/10.1007/s12046-017-0654-4>.
- [8] L. Wang, J. Lu, Y. Li, T. Yahagi, T. Okamoto, Noise removal for medical X-ray images in wavelet domain, *Electr. Eng. Japan (English Transl. Denki Gakkai Ronbunshi)* 163 (3) (2008) 37–46, <https://doi.org/10.1002/eej.20486>.
- [9] J. Zhang, L. Zhao, Z. Wei, Poisson-Skellam distribution based regularization conditional random field method for photon-limited Poisson image denoising, *Signal Processing* 188 (2021), 108165, <https://doi.org/10.1016/j.sigpro.2021.108165>.
- [10] A. Kumar, P. Kumar, S. Srivastava, A skewness reformed complex diffusion based unsharp masking for the restoration and enhancement of Poisson noise corrupted mammograms, *Biomed. Signal Process. Control* 73 (2022), 103421, <https://doi.org/10.1016/j.bspc.2021.103421>.
- [11] T.B. Chandra, K. Verma, Analysis of quantum noise-reducing filters on chest X-ray images: a review, *Meas. J. Int. Meas. Confed.* 153 (2020), <https://doi.org/10.1016/j.measurement.2019.107426>.
- [12] K.V. Thakur, O.H. Damodare, A.M. Sapkal, Poisson noise reducing bilateral filter, *Procedia Comput. Sci.* 79 (2016) 861–865, <https://doi.org/10.1016/j.procs.2016.03.087>.
- [13] F. Latifoğlu, A novel approach to speckle noise filtering based on Artificial Bee Colony algorithm: an ultrasound image application, *Comput. Methods Programs Biomed.* 111 (3) (2013) 561–569, <https://doi.org/10.1016/j.cmpb.2013.05.009>.
- [14] J.S. Lim, *Two-dimensional signal and image processing*, Prentice Hall, Englewood Cliffs, NJ, 1990.
- [15] C.V. Cannistraci, F.M. Montevicchi, M. Alessio, Median-modified Wiener filter provides efficient denoising, preserving spot edge and morphology in 2-DE image processing, *Proteomics* 9 (21) (2009) 4908–4919, <https://doi.org/10.1002/pmic.200800538>.
- [16] C. Park, Y. Lee, Application feasibility of median modified Wiener filter (MMWF) algorithm for customized breast ACR phantom images using 3D printing technology in mammography, *Nucl. Instruments Methods Phys. Res. Sect. A Accel. Spectrometers, Detect. Assoc. Equip.* 1031 (2022), 166570, <https://doi.org/10.1016/j.nima.2022.166570>.
- [17] C.R. Park, S.H. Kang, Y., modified wiener filter for improving the image quality of gamma camera images Lee, "Median modified wiener filter for improving the image quality of gamma camera images", *Nucl. Eng. Technol.* 52 (10) (2020) 2328–2333, <https://doi.org/10.1016/j.net.2020.03.022>.
- [18] H.W. Xie, H. Guo, G.Q. Zhou, N.Q. Nguyen, R.W. Prager, Improved ultrasound image quality with pixel-based beamforming using a Wiener-filter and a SNR-dependent coherence factor, *Ultrasonics* 119 (2022), 106594, <https://doi.org/10.1016/j.ultras.2021.106594>.
- [19] T. Meraj, et al., Lung nodules detection using semantic segmentation and classification with optimal features, *Neural Comput. Appl.* 33 (17) (2021) 10737–10750, <https://doi.org/10.1007/s00521-020-04870-2>.
- [20] D. Using and P. Feature, "Detection Using Parallel Feature Fusion," pp. 1–20, 2021.
- [21] T. Meraj, et al., A quantization assisted U-Net study with ICA and deep features fusion for breast cancer identification using ultrasonic data, *PeerJ Comput. Sci.* 7 (2021) 1–28, <https://doi.org/10.7717/PEERJ-CS.805>.
- [22] P.H. Dinh, A novel approach based on Grasshopper optimization algorithm for medical image fusion, *Expert Syst. Appl.* 171 (2021), 114576, <https://doi.org/10.1016/j.eswa.2021.114576>.
- [23] P.H. Dinh, Multi-modal medical image fusion based on equilibrium optimizer algorithm and local energy functions, *Appl. Intell.* 51 (11) (2021) 8416–8431, <https://doi.org/10.1007/s10489-021-02282-w>.
- [24] P.H. Dinh, Combining Gabor energy with equilibrium optimizer algorithm for multi-modality medical image fusion, *Biomed. Signal Process. Control* 68 (2021), 102696, <https://doi.org/10.1016/j.bspc.2021.102696>.
- [25] P.H. Dinh, A novel approach based on Three-scale image decomposition and Marine predators algorithm for multi-modal medical image fusion, *Biomed. Signal Process. Control* 67 (2021), 102536, <https://doi.org/10.1016/j.bspc.2021.102536>.

- [26] P.H. Dinh, An improved medical image synthesis approach based on marine predators algorithm and maximum Gabor energy, *Neural Comput. Appl.* 34 (6) (2022) 4367–4385, <https://doi.org/10.1007/s00521-021-06577-4>.
- [27] P.H. Dinh, A novel approach using structure tensor for medical image fusion, *Multidimens. Syst. Signal Process.* (2022), <https://doi.org/10.1007/s11045-022-00829-9>.
- [28] P.H. Dinh, N.L. Giang, A new medical image enhancement algorithm using adaptive parameters, *Int. J. Imaging Syst. Technol.* (2022) 1–21, <https://doi.org/10.1002/ima.22778>.
- [29] C. Huerga, et al., Role of correlated noise in textural features extraction, *Phys. Medica* 91 (2021) 87–98, <https://doi.org/10.1016/j.ejmp.2021.10.015>.
- [30] P. Subbuthai, K. Kavithabharathi, S. Muruganand, Reduction of types of Noises in dental Images, *Int. J. Comput. Appl. Technol. Res.* 2 (4) (2013) 436–442, <https://doi.org/10.7753/ijcatr0204.1009>.
- [31] C. Tomasi, R. Manduchi, Bilateral filtering for gray and color images, *Proc. IEEE Int. Conf. Comput. Vis.* (1998) 839–846, <https://doi.org/10.1109/iccv.1998.710815>.
- [32] M. A. Asim, M. U. Akram, and A. A. Salam, “Comparison of different de-noising techniques for removal of poison noise from cervical X-Rays images,” *Proc. 2017 Int. Conf. Commun. Comput. Digit. Syst. C-CODE 2017*, pp. 281–286, 2017, doi: 10.1109/C-CODE.2017.7918943.
- [33] A. Buades, B. Coll, and J. M. Morel, “A non-local algorithm for image denoising,” *Proc. - 2005 IEEE Comput. Soc. Conf. Comput. Vis. Pattern Recognition, CVPR 2005*, vol. II, no. 0, pp. 60–65, 2005, doi: 10.1109/CVPR.2005.38.
- [34] P. Irrera, I. Bloch, and M. Delplanque, “Contrast enhancement of Micro Dose X-RAY images,” *2014 IEEE 11th Int. Symp. Biomed. Imaging, ISBI 2014*, no. June 2014, pp. 489–492, 2014, doi: 10.1109/isbi.2014.6867915.
- [35] K. He, J. Sun, X. Tang, Guided image filtering, *IEEE Trans. Pattern Anal. Mach. Intell.* 35 (6) (2013) 1397–1409, <https://doi.org/10.1109/TPAMI.2012.213>.
- [36] X. Zhang, C. He, Robust double-weighted guided image filtering, *Signal Processing* 199 (2022), 108609, <https://doi.org/10.1016/j.sigpro.2022.108609>.
- [37] S.G. Chang, B. Yu, M. Vetterli, Adaptive wavelet thresholding for image denoising and compression, *IEEE Trans. Image Process.* 9 (9) (2000) 1532–1546, <https://doi.org/10.1109/83.862633>.
- [38] S. Routray, A.K. Ray, C. Mishra, Image denoising by preserving geometric components based on weighted bilateral filter and curvelet transform, *Optik (Stuttg)* 159 (2018) 333–343, <https://doi.org/10.1016/j.jpleo.2018.01.096>.
- [39] L. Wang, J. Lu, Y. Li, T. Yahagi, T. Okamoto, Noise reduction using wavelet with application to medical X-ray image, *Proc. IEEE Int. Conf. Ind. Technol.* (2005) 33–38, <https://doi.org/10.1109/ICIT.2005.1600606>.
- [40] L. Du, Y. Wen, and J. Ma, “Dual tree complex wavelet transform and Bayesian estimation based denoising of poisson-corrupted X-ray images,” *Proc. 2013 Int. Conf. Intell. Control Inf. Process. ICICIP 2013*, pp. 598–603, 2013, doi: 10.1109/ICICIP.2013.6568145.
- [41] R.J. Ferrari, R. Winsor, Digital radiographic image denoising via wavelet-based hidden Markov model estimation, *J. Digit. Imaging* 18 (2) (2005) 154–167, <https://doi.org/10.1007/s10278-004-1908-3>.
- [42] F. Luisier, C. Vonesch, T. Blu, M. Unser, Fast interscale wavelet denoising of Poisson-corrupted images, *Signal Processing* 90 (2) (2010) 415–427, <https://doi.org/10.1016/j.sigpro.2009.07.009>.
- [43] D.N.H. Thanh, V.B.S. Prasath, L.M. Hieu, A review on CT and X-ray images denoising methods, *Inform.* 43 (2) (2019) 151–159, <https://doi.org/10.31449/inf.v43i2.2179>.
- [44] K. Dabov, A. Foi, V. Katkovnik, K. Egiazarian, “Image denoising with block-matching and 3D filtering”, *image process. algorithms syst. neural networks*, Mach. Learn. 6064 (2006) 606414, <https://doi.org/10.1117/12.643267>.
- [45] Q. Chen, D. Wu, Image denoising by bounded block matching and 3D filtering, *Signal Processing* 90 (9) (2010) 2778–2783, <https://doi.org/10.1016/j.sigpro.2010.03.016>.
- [46] S. Lee, M.G. Kang, Poisson-Gaussian noise reduction for X-ray images based on local linear minimum mean square error shrinkage in nonsubsampling contourlet transform domain, *IEEE Access* 9 (2021) 100637–100651, <https://doi.org/10.1109/ACCESS.2021.3097078>.
- [47] N.Kingsbury, “The dual-tree complex wavelet transform: a new efficient tool for image restoration and enhancement,” 1998.
- [48] B. Zhang, M.J. Fadili, J.L. Starck, “Multi-scale variance stabilizing transform for multi-dimensional poisson count image denoising”, *ICASSP, IEEE Int. Conf. Acoust. Speech Signal Process.* - Proc. 2 (2006) 81–84, <https://doi.org/10.1109/icassp.2006.1660284>.
- [49] M. Niknejad and M. A. T. Figueiredo, “Poisson image denoising using best linear prediction: A post-processing framework,” *Eur. Signal Process. Conf.*, vol. 2018-Septe, no. 2, pp. 2230–2234, 2018, doi: 10.23919/EUSIPCO.2018.853220.
- [50] N. H. Hai, D. N. H. Thanh, N. N. Hien, C. Premachandra, and V. B. S. Prasath, “A fast denoising algorithm for X-ray images with variance stabilizing transform,” *Proc. 2019 11th Int. Conf. Knowl. Syst. Eng. KSE 2019*, pp. 8–12, 2019, doi: 10.1109/KSE.2019.8919364.
- [51] C. Tian, L. Fei, W. Zheng, Y. Xu, W. Zuo, C.W. Lin, Deep learning on image denoising: an overview, *Neural Networks* 131 (2020) 251–275, <https://doi.org/10.1016/j.neunet.2020.07.025>.
- [52] D.L. Donoho, Compressed sensing, *IEEE Trans. Inf. Theory* 52 (4) (2006) 1289–1306, <https://doi.org/10.1109/TIT.2006.871582>.
- [53] Z. Zhang, Y. Xu, J. Yang, X. Li, D. Zhang, A survey of sparse representation: algorithms and applications, *IEEE Access* 3 (2015) 490–530, <https://doi.org/10.1109/ACCESS.2015.2430359>.
- [54] Q. Li, W. Wang, G. Chen, D. Zhao, Medical image fusion using segment graph filter and sparse representation, *Comput. Biol. Med.* 131 (2021), 104239, <https://doi.org/10.1016/j.compbiomed.2021.104239>.
- [55] H. Li and F. Liu, “Image denoising via sparse and redundant representations over learned dictionaries in wavelet domain,” *Proc. 5th Int. Conf. Image Graph. ICIG 2009*, vol. 15, no. 12, pp. 754–758, 2009, doi: 10.1109/ICIG.2009.101.
- [56] R. Giryes, M. Elad, Sparsity-based poisson denoising with dictionary learning, *IEEE Trans. Image Process.* 23 (12) (2014) 5057–5069, <https://doi.org/10.1109/TIP.2014.2362057>.
- [57] H. Takeda, S. Farsiu, P. Milanfar, Kernel regression for image processing and reconstruction, *IEEE Trans. Image Process.* 16 (2) (2007) 349–366, <https://doi.org/10.1109/TIP.2006.888330>.
- [58] S. Zhu, Z. Yu, Self-guided filter for image denoising, *IET Image Process.* 14 (11) (2020) 2561–2566, <https://doi.org/10.1049/iet-ipr.2019.1471>.
- [59] I. Congress, S. Processing, F. Ri, Q. Dqg, R. V. W. Dqg, and P. Molqohxqj, “6Wdfnhg ` Hqrlvlqj \$ Xwrhqrghu Dqg ` Ursrxw 7Rjhkwku Wr 3Uyhqw 2Yhuilwqlj L ` Hhs 1Hxudo,” no. Cisp, pp. 697–701, 2015.
- [60] X.J. Mao, C. Shen, Y. Bin Yang, Image restoration using very deep convolutional encoder-decoder networks with symmetric skip connections, *Adv. Neural Inf. Process. Syst. no. Nips* (2016) 2810–2818.
- [61] K. Zhang, W. Zuo, Y. Chen, D. Meng, L. Zhang, Beyond a Gaussian denoiser: Residual learning of deep CNN for image denoising, *IEEE Trans. Image Process.* 26 (7) (2017) 3142–3155, <https://doi.org/10.1109/TIP.2017.2662206>.
- [62] X. Jia, X. Feng, S. Liu, Dual non-autonomous deep convolutional neural network for image denoising, *Inf. Sci. (Ny)* 572 (2021) 263–276, <https://doi.org/10.1016/j.ins.2021.05.001>.
- [63] Z. Lyu, Y. Chen, Y. Hou, C. Zhang, NSTBNet: Toward a nonsubsampling shearlet transform for broad convolutional neural network image denoising, *Digit. Signal Process. A Rev. J.* 123 (2022), 103407, <https://doi.org/10.1016/j.dsp.2022.103407>.
- [64] H. Song, et al., Denoising of MR and CT images using cascaded multi-supervision convolutional neural networks with progressive training, *Neurocomputing* 469 (2022) 354–365, <https://doi.org/10.1016/j.neucom.2020.10.118>.
- [65] A.A. Bindilatti, M.A.C. Vieira, N.D.A. Mascarenhas, Poisson Wiener filtering with non-local weighted parameter estimation using stochastic distances, *Signal Processing* 144 (2018) 68–76, <https://doi.org/10.1016/j.sigpro.2017.10.001>.
- [66] Y. Fan, J. Liu, R. Yao, X. Yuan, COVID-19 Detection from X-ray images using multi-kernel-size spatial-channel attention network, *Pattern Recognition* 119 (2021), 108055, <https://doi.org/10.1016/j.patcog.2021.108055>.
- [67] Gonzales R., Woods, R. “Digital Image Processing”, 2002 by Prentice-Hall, Inc. Upper Saddle River, New Jersey 07458.
- [68] Sxeliski, R., “Computer Vision: Algorithms and Applications.” September 3, 2010 draft 2010 Springer. Electronics Letters, IEE, Vol. 23, pp. 131 .
- [69] A. E. Cetin and R. Ansari, “Iterative procedure for designing two dimensional FIR filters”, *Electronics Letters, IEE*, Vol. 23, pp.
- [70] M. Rafati, F. Farnia, M.E. Taghvaei, A.M. Nickfarjam, Fuzzy genetic-based noise removal filter for digital panoramic X-ray images, *Biocybern. Biomed. Eng.* 38 (4) (2018) 941–965, <https://doi.org/10.1016/j.bbe.2018.08.005>.
- [71] R. Eberhart, J.K. Sixth, A new optimizer using particle swarm theory, *Proc. IEEE Symp. Micro Mach. Hum. Sci. Nagoys, Japan, 1997*, pp. 39–43.
- [72] K. J. and L. G. , Geom ZW, “A new heuristic optimization algorithm: Harmony search. Simulation,” vol. 76, pp. 60–68, 2001.
- [73] J. H. Holland, “Adaptation in Natural and Artificial Systems .,” *MIT Press.*, p. 1975, 1975.
- [74] D. Karaboga, “AN IDEA BASED ON HONEY BEE SWARM FOR NUMERICAL OPTIMIZATION”, *Tech. REPORT-TRO6 Erciyes Univ, Eng. Fac. Comput. Eng. Dep. Kayseri/Türkiye* (2005).
- [75] W. Zhao, L. Wang, Z. Zhang, Atom search optimization and its application to solve a hydrogeologic parameter estimation problem, *Knowledge-Based Syst.* 163 (2019) 283–304, <https://doi.org/10.1016/j.knsys.2018.08.030>.
- [76] A. Faramarzi, M. Heidarinejad, B. Stephens, S. Mirjalili, Equilibrium optimizer: a novel optimization algorithm, *Knowledge-Based Syst.* 191 (2020), 105190, <https://doi.org/10.1016/j.knsys.2019.105190>.
- [77] S. Saremi, S. Mirjalili, A. Lewis, Grasshopper optimisation algorithm: theory and application, *Adv. Eng. Softw.* 105 (2017) 30–47, <https://doi.org/10.1016/j.advengsoft.2017.01.004>.
- [78] A. Faramarzi, M. Heidarinejad, S. Mirjalili, A.H. Gandomi, Marine Predators Algorithm: a nature-inspired metaheuristic, *Expert Syst. Appl.* 152 (2020), 113377, <https://doi.org/10.1016/j.eswa.2020.113377>.
- [79] A. Askarzadeh, A novel metaheuristic method for solving constrained engineering optimization problems: crow search algorithm, *Comput. Struct.* 169 (2016) 1–12, <https://doi.org/10.1016/j.compstruc.2016.03.001>.
- [80] S. T. A. Alan C. Bovik, *Basic Linear Filtering with Application to Image Enhancement*. 2009.
- [81] T.S. Huang, G.J. Yang, G.Y. Tang, A Fast Two-Dimensional Median Filtering Algorithm, *IEEE Trans. Acoust.* 27 (1) (1979) 13–18, <https://doi.org/10.1109/TASSP.1979.1163188>.
- [82] S. Rawat, K.P.S. Rana, V. Kumar, A novel complex-valued convolutional neural network for medical image denoising, *Biomed. Signal Process. Control* 69 (2021), 102859, <https://doi.org/10.1016/j.bspc.2021.102859>.



# BIOMEDICAL SIGNAL PROCESSING AND CONTROL

## Editor-in-Chief

**Panayiotis Kyriacou**  
Sch. of Engineering & Math. Sciences,  
City, University of London,  
10 Northampton Square, EC1V 0HB,  
London, UK

## Founding Editor

**R. Allen**  
University of Southampton,  
Southampton

## Associate Editors

**M. Baumert**  
The University of Adelaide,  
Adelaide, Australia

### **F. Chen (Felix)**

Southern University of Science and Technology Department of Electrical and Electronic Engineering, Shenzhen, China

### **Martin Oswaldo Mendez Garcia**

Autonomous University of San Luis Potosi, San Luis Potosi, Mexico

### **R.B. Pachori**

IIT Indore,  
Indore, India

### **G. Sannino**

Institute for High Performance Computing and Networking National Research Council,  
Naples, Italy

### **Dr. Shanshan(Sophia) Wang**

Paul C. Lauterbur Research Center for Biomedical Imaging  
Shenzhen Institutes of Advanced Technology  
Chinese Academy of Sciences  
1068 Xueyuan Avenue, Shenzhen University Town, Shenzhen, China  
E-mail Address: Sophiasswang@hotmail.com

### **M. Zervakis**

Technical University of Crete,  
Crete, Greece

### **Y-D. Zhang**

University of Leicester Department of Informatics, Leicester, United Kingdom

## Editorial Advisory Board

**M. Akay**, University of Houston, Houston, Texas, USA

**A. M. Bianchi**, Politecnico di Milano, Milan, Italy

**U. Bracale**, Università Federico II di Napoli, Italy

**S. Cerutti**, Politecnico di Milano, Milan, Italy

**G. Chase**, University of Canterbury, Christchurch, New Zealand

**F. Chen**, Southern University of Science and Technology, China

**A. Cichocki**, Skolkovo Institute of Science and Technology (SKOLTECH), Moscow, Russia

**J.W. Clark**, Rice University, Houston, Texas, USA

**J. Escudero**, University of Edinburgh, Edinburgh, UK

**D. Feng**, The University of Sydney, Sydney, New South Wales, Australia

**D.D. Feng**, University of Sydney, Australia

**G. Giakos**, Manhattan College, New York, USA

**D. K. Kumar**, RMIT University, Melbourne, Australia

**C. Manfredi**, Università degli Studi di Firenze, Firenze, Italy

**R. Merletti**, Politecnico di Torino, Torino, Italy

**A. van Oosterom**, University of Nijmegen, Nijmegen, The Netherlands

**M. Paolo**, University of Campania Luigi Vanvitelli, Italy

**C. Pattichis**, University of Cyprus, Nicosia, Cyprus

**P. Ramaswamy**, University of Kent, Kent, UK

**F. Schlindwein**, University of Leicester, Leicester, UK

**D. Simpson**, University of Southampton, Southampton, UK

**T. Sinkjaer**, Danish National Research Foundation, Copenhagen, Denmark

**L. Sörnmo**, Lund University, Lund, Sweden

**R. Stagni**, Università degli studi di Bologna, Italy

**L. Xu**, Beihang University, China

**J. Yu**, Fudan University, China

**Y.-D. (Eugene) Zhang**, University of Leicester

**Y. Zhou**, Shenzhen University, China



Already have a manuscript?

Use our Manuscript Matcher to find the best relevant journals!

[Find a Match](#)

Filters

[Clear All](#)

Web of Science Coverage

Open Access

Category

Country / Region

Language

Frequency

## Refine Your Search Results

Biomedical Signal Processing and Control

[Search](#)

Sort By: Relevancy

### Search Results

Found 11,512 results (Page 1)

[Share These Results](#)

### Exact Match Found

**BIOMEDICAL SIGNAL PROCESSING AND CONTROL**

Publisher: **ELSEVIER SCI LTD , THE BOULEVARD, LANGFORD LANE, KIDLINGTON, OXFORD, ENGLAND, OXON, OX5 1GB**

ISSN / eISSN: **1746-8094 / 1746-8108**

Web of Science Core Collection: **Science Citation Index Expanded**

Additional Web of Science Indexes: **Current Contents Engineering, Computing & Technology | Essential Science Indicators**

[Share This Journal](#)

[View profile page](#)

\* Requires free login.

# 2022 Journal Performance Data for: Biomedical Signal Processing and Control

ISSN

1746-8094

EISSN

1746-8108

JCR ABBREVIATION

BIOMED SIGNAL PROCES

ISO ABBREVIATION

Biomed. Signal Process.  
Control

## Journal Information

EDITION

Science Citation Index  
Expanded (SCIE)

CATEGORY

ENGINEERING, BIOMEDICAL -  
SCIE

LANGUAGES

English

REGION

ENGLAND

1ST ELECTRONIC JCR YEAR

2008

## Publisher Information

PUBLISHER

ELSEVIER SCI LTD

ADDRESS

THE BOULEVARD, LANGFORD  
LANE, KIDLINGTON, OXFORD  
OX5 1GB, OXON, ENGLAND

PUBLICATION FREQUENCY

8 issues/year

## Rank by Journal Impact factor

Journals within a category are sorted in descending order by Journal Impact Factor (JIF) resulting in the Category Ranking below. A separate rank is shown for each category in which the journal is listed in JCR. Data for the most recent year is presented at the top of the list, with other years shown in reverse chronological order. [Learn more](#)

### EDITION

#### Science Citation Index Expanded (SCIE)

##### CATEGORY

ENGINEERING, BIOMEDICAL

**26/96**

JCR YEAR	JIF RANK	QUART ILE	JIF PERCENTILE	
2022	26/96	Q2	73.4	
2021	30/98	Q2	69.90	
2020	34/89	Q2	62.36	
2019	32/87	Q2	63.79	
2018	27/80	Q2	66.88	
2017	25/78	Q2	68.59	
2016	33/77	Q2	57.79	
2015	47/76	Q3	38.82	
2014	48/76	Q3	37.50	
2013	40/76	Q3	48.03	
2012	59/79	Q3	25.95	
2011	53/72	Q3	27.08	
2010	54/70	Q4	23.57	
2009	52/59	Q4	12.71	
2008	48/52	Q4	8.65	

### EDITION

#### Science Citation Index Expanded (SCIE)

##### CATEGORY

MEDICAL LABORATORY TECHNOLOGY

**N/A**

JCR YEAR	JIF RANK	QUART ILE	JIF PERCENTILE	
2022	N/A	N/A	N/A	
2021	N/A	N/A	N/A	
2020	N/A	N/A	N/A	
2019	N/A	N/A	N/A	
2018	N/A	N/A	N/A	
2017	9/30	Q2	71.67	
2016	14/30	Q2	55.00	
2015	20/30	Q3	35.00	
2014	15/30	Q2	51.67	
2013	16/31	Q3	50.00	
2012	20/32	Q3	39.06	
2011	20/32	Q3	39.06	
2010	22/31	Q3	30.65	
2009	24/29	Q4	18.97	
2008	23/27	Q4	16.67	





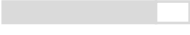
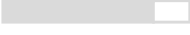
## Rank by Journal Citation Indicator (JCI)

Journals within a category are sorted in descending order by Journal Citation Indicator (JCI) resulting in the Category Ranking below. A separate rank is shown for each category in which the journal is listed in JCR. Data for the most recent year is presented at the top of the list, with other years shown in reverse chronological order. [Learn more](#)

### CATEGORY

ENGINEERING, BIOMEDICAL

**31/116**

JCR YEAR	JCI RANK	QUARTILE	JCI PERCENTILE	
2022	31/116	Q2	73.71	
2021	30/115	Q2	74.35	
2020	26/106	Q1	75.94	
2019	23/105	Q1	78.57	
2018	19/103	Q1	82.04	
2017	20/101	Q1	80.69	





# Biomedical Signal Processing and Control

Supports open access

8.2  
CiteScore

5.1  
Impact Factor

Articles & Issues

About

Publish

Order journal

Search in this journal

Submit your article

Guide for authors

## Volume 79, Part 1

January 2023

Download full issue

< Previous vol/issue

Next vol/issue >

### Actions for selected articles

Select all / Deselect all

Download PDFs

Receive an update when the latest issues in this journal are published

Sign in to set up alerts

FEEDBACK

## Biomedical Signal Processing and Control

Supports open access

Submit your article

Articles & Issues

About

Publish

Order journal

Search in this journal

Guide for authors

Article preview

### Actions for selected articles

Select all / Deselect all

Download PDFs

Export citations

Show all article previews

Research article / Abstract only

A novel method based on Wiener filter for denoising Poisson noise from medical X-Ray images

Volkan Göreke

Article 104031

Article preview